



# Early Science with the Large Millimeter Telescope: An Energy-driven Wind Revealed by Massive Molecular and Fast X-Ray Outflows in the Seyfert Galaxy IRAS 17020+4544

A. L. Longinotti<sup>1,2</sup> , O. Vega<sup>1</sup> , Y. Krongold<sup>3</sup> , I. Aretxaga<sup>1</sup> , M. Yun<sup>4</sup> , V. Chavushyan<sup>1</sup> , C. Feruglio<sup>5</sup> , A. Gómez-Ruiz<sup>1,2</sup> , A. Montaña<sup>1,2</sup> , J. León-Tavares<sup>6</sup> , A. Olguín-Iglesias<sup>1</sup> , M. Giroletti<sup>7</sup> , M. Guainazzi<sup>8</sup> , J. Kotilainen<sup>9,10</sup> , F. Panessa<sup>11</sup> , L. A. Zapata<sup>12</sup> , I. Cruz-Gonzalez<sup>3</sup> , V. M. Patiño-Álvarez<sup>13</sup> , D. Rosa-Gonzalez<sup>1</sup> , A. Carramiñana<sup>1</sup> , L. Carrasco<sup>1</sup> , E. Costantini<sup>14</sup> , D. Dultzin<sup>3</sup> , J. Guichard<sup>1</sup> , I. Puerari<sup>1</sup> , and M. Santos-Lleo<sup>15</sup>

<sup>1</sup> Instituto Nacional de Astrofísica, Óptica y Electrónica, Luis E. Erro 1, Tonantzintla, Puebla, C.P. 72840, México; [annalia@inaoep.mx](mailto:annalia@inaoep.mx)

<sup>2</sup> CONACyT-INAOE

<sup>3</sup> Instituto de Astronomía, Universidad Nacional Autónoma de México, Circuito Exterior, Ciudad Universitaria, Ciudad de México 04510, México

<sup>4</sup> Department of Astronomy, University of Massachusetts, MA 01003, USA

<sup>5</sup> INAF Osservatorio Astronomico di Trieste, Via G. Tiepolo 11, Trieste, Italy

<sup>6</sup> Centre for Remote Sensing and Earth Observation Processes (TAP), Flemish Institute for Technological Research (VITO), Boeretang 282, B-2400 Mol, Belgium

<sup>7</sup> INAF Istituto di Radioastronomia, via Gobetti 101, I-40129, Bologna, Italy

<sup>8</sup> European Space Agency, European Space Research & Technology Centre (ESTEC), Postbus 299, 2200 AG Noordwijk, The Netherlands

<sup>9</sup> Finnish Centre for Astronomy with ESO (FINCA), University of Turku, Finland

<sup>10</sup> Department of Physics and Astronomy, University of Turku, Finland

<sup>11</sup> Istituto di Astrofisica e Planetologia Spaziali di Roma (IAPS), Via del Fosso del Cavaliere 100, I-00133 Roma, Italy

<sup>12</sup> Instituto de Radioastronomía y Astrofísica, Universidad Nacional Autónoma de México, P.O. Box 3-72, 58090, Morelia, Michoacán, México

<sup>13</sup> Max-Planck-Institut für Radioastronomie, Auf dem Hügel 69, D-53121 Bonn, Germany

<sup>14</sup> SRON, Netherlands Institute for Space Research, Sorbonnelaan 2, 3584 CA Utrecht, The Netherlands

<sup>15</sup> European Space Agency—ESAC, P.O. Box, 78 E-28691 Villanueva de la Cañada, Madrid, Spain

Received 2018 August 2; revised 2018 September 26; accepted 2018 October 3; published 2018 October 29

## Abstract

We report on the coexistence of powerful gas outflows observed in millimeter and X-ray data of the radio-loud narrow-line Seyfert 1 Galaxy IRAS 17020+4544. Thanks to the large collecting power of the Large Millimeter Telescope (LMT), a prominent line arising from the <sup>12</sup>CO(1–0) transition was revealed in recent observations of this source. The complex profile is composed by a narrow double-peak line and a broad wing. While the double-peak structure may be arising in a disk of molecular material, the broad wing is interpreted as the signature of a massive outflow of molecular gas with an approximate bulk velocity of  $-660 \text{ km s}^{-1}$ . This molecular wind is likely associated to a multi-component X-ray ultra-fast outflow with velocities reaching up to  $\sim 0.1c$  and column densities in the range  $10^{21-23.9} \text{ cm}^{-2}$  that was reported in the source prior to the LMT observations. The momentum load estimated in the two gas phases indicates that within the observational uncertainties the outflow is consistent with being propagating through the galaxy and sweeping up the gas while conserving its energy. This scenario, which has been often postulated as a viable mechanism of how active galactic nucleus (AGN) feedback takes place, has so far been observed only in ultraluminous infrared galaxy sources. IRAS 17020+4544 with bolometric and infrared luminosity, respectively, of  $5 \times 10^{44} \text{ erg s}^{-1}$  and  $1.05 \times 10^{11} L_{\odot}$  appears to be an example of AGN feedback in a NLSy1 Galaxy (a low power AGN). New proprietary multi-wavelength data recently obtained on this source will allow us to corroborate the proposed hypothesis.

*Key words:* galaxies: Seyfert – infrared: galaxies

## 1. Introduction

Feedback from luminous active galactic nuclei (AGNs) is widely recognized as a key ingredient for evolution of galaxies (Di Matteo et al. 2005; Hopkins & Elvis 2010). The energy released as a result of the accretion of large amount of gas during the earliest stage of a quasar’s life acts as a trigger for the ejection of powerful outflows driven by the AGN. The action of such winds would be to sweep the gas and possibly eject it out of the host galaxy, thus providing an effective mechanism of quenching star formation.

One of the most credited scenarios for explaining how quasar feedback actually works proposes that a subrelativistic wind, with velocity higher than  $10^4 \text{ km s}^{-1}$  and typically observable in the X-ray band, is launched at accretion disk scale (Faucher-Giguère & Quataert 2012). This highly ionized X-ray gas is currently observed in the form of ultra-fast outflows in 30%–40% of AGN spectra (Tombesi et al. 2012; Gofford et al. 2013).

While traveling outward, the wind undergoes a collision with the interstellar medium (ISM) that gives rise to shock processes

(King 2010). After shocking with the gas, deceleration and cooling processes take place in the outflow, which keeps moving outward giving rise to less ionized lines, observable in the optical band (e.g., Harrison et al. 2014; Carniani et al. 2015; Fiore et al. 2017), and to the formation of a bubble of hot tenuous gas (e.g., Zubovas & King 2012). At even larger scales, the effect of the cooling eventually converts the ionized gas to a colder phase medium outflowing at a much lower velocity. This latest phase is frequently observed in several ultraluminous infrared galaxies (ULIRGs) and quasars (Feruglio et al. 2010, 2015; Veilleux et al. 2013; Cicone et al. 2014).

The outflow properties can be described in term of mass loss rate ( $\dot{M}_{\text{out}}$ ), outflow velocity ( $v_{\text{out}}$ ), and momentum flux ( $\dot{M}_{\text{out}} \times v_{\text{out}}$ ). The nuclear wind at launching radius carries an amount of energy equal to  $\frac{1}{2} \dot{M}_{\text{nuc1}} \times v_{\text{nuc1}}^2$ . If during the expansion the outflow conserves most of its initial energy, the energy conservation for the large-scale outflow leads to  $\dot{M}_{\text{ls}} \times v_{\text{ls}}^2 = \dot{M}_{\text{nuc1}} \times v_{\text{nuc1}}^2$ . The resulting momentum flux of the

wind at large scale is then boosted by a factor proportional to the ratio of the outflow velocities  $\dot{P}_{\text{ls}} = \frac{v_{\text{nucl}}}{v_{\text{ls}}} \times \dot{P}_{\text{nucl}}$ . These considerations lead to a characteristic prediction for energy-conserving outflows that are driven by a nuclear wind whose momentum rate is comparable to the AGN radiative power  $\dot{P}_{\text{nucl}} = \frac{L_{\text{AGN}}}{c}$  (see Figure 5 in Faucher-Giguère & Quataert 2012, or Figure 1 in Nardini & Zubovas 2018).

If instead the energy of the nuclear wind is dissipated, the momentum rate of the large-scale wind does not receive any “boosting factor,” meaning that  $\dot{P}_{\text{ls}} = \dot{P}_{\text{nucl}}$ , i.e., the momentum rate at launching radius, is equal to the momentum rate at large scale. In this case, the expansion of the wind follows the prediction of momentum conservation.

To test and corroborate the fascinating hypothesis of a multi-phase outflow spanning the galaxy at all scales, it is evident that observations have to target as many outflow components as possible in the same object. This may be expensive in terms of observational campaigns: for example, the innermost X-ray phase of the wind is not easily detectable in the majority of X-ray spectra, the extended emission of hot gas is too tenuous to be observed in a reasonable amount of telescope time, or the source of interest is at too high of a redshift to allow fine spatially resolved spectroscopy.

To date, only two cases of ULIRGS have been published where the X-ray and molecular phases of the outflow were observed and physically related (Feruglio et al. 2015; Tombesi et al. 2015). Remarkably, both results are in excellent agreement with the prediction of the energy-conserving outflow model outlined above (but see Nardini & Zubovas 2018 for a recent reassessment of both results).

In this Letter, we report on a multi-phase outflow discovered in the radio-loud narrow-line Seyfert 1 galaxy IRAS 17020+4544 (Wisotzki & Bade 1997; Doi et al. 2011), which was observed in the X-ray (Longinotti et al. 2015), radio band (Giroletti et al. 2017) and molecular gas (this Letter). Even at the moderate luminosity of this source ( $5 \times 10^{44} \text{ erg s}^{-1}$ ), the emerging picture is stunningly coherent with the action of an AGN-driven outflow capable of propagating through the galaxy at all scales. The cosmological parameters adopted throughout this Letter are  $H_0 = 70 \text{ km s}^{-1} \text{ Mpc}^{-1}$ ,  $\Omega_m = 0.3$ ,  $\Omega_\Lambda = 0.7$ . At the redshift of the source,  $z = 0.0604$ , the spatial scale of  $1''$  corresponds to a physical scale of 1.1 kpc and the luminosity distance is 250 Mpc.

## 2. The Data: the Large Millimeter Telescope (LMT)

Observations were obtained at the LMT Alfonso Serrano, located on the Sierra Negra Volcano in Mexico, at an elevation of 4600 m (Hughes et al. 2010), using the Redshift Search Receiver instrument (RSR; Erickson et al. 2007). The observing run was carried out in six different nights between 2015 May and June, as part of an Early Science program addressed to study the molecular emission of a wide sample of AGNs (P.I.: J. León-Tavares). During this phase, only the inner 32.5 m diameter section of the telescope surface was illuminated, leading to an effective beam size of 20 arcsec at 110 GHz.

The RSR has four pixels arranged in a dual beam, dual polarization configuration, and four broadband receivers that instantaneously cover the frequency range 73–111 GHz with a spectral resolution of 31 MHz ( $R = 3000$  or  $100 \text{ km s}^{-1}$  at 93 GHz).

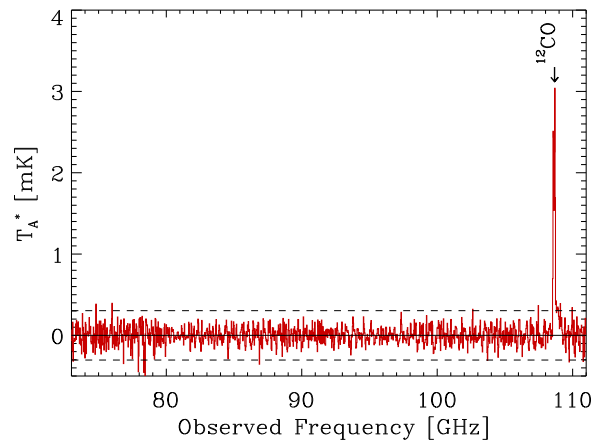


**Figure 1.** RSR spectrum of the  $^{12}\text{CO}(1-0)$  line in IRAS 17020+4544 obtained with the LMT telescope. The baseline was already subtracted and the horizontal dashed lines mark the  $3\sigma$  threshold. The arrow marks the frequency of the  $^{12}\text{CO}(1-0)$  line at the redshift of IRAS 17020+4544.

IRAS 17020+4544 was observed for a total of 525 minutes in this configuration over the observing nights, with  $T_{\text{sys}}$  ranging between  $\sim 100$  to 123 K and  $\tau_{225 \text{ GHz}}$  ranging between 0.2 and 0.4. Telescope pointing was checked every 60–90 minutes by observing the source 3C 345. The pointing corrections were always less than 5 arcsec. The focus was also checked and corrected at the beginning of each run and during sunsets and sunrises. The observations were calibrated and processed using the latest version of Data Reduction and Analysis Methods in Python (DREAMPY), a software package written by G. Narayanan for the purposes of calibrating and reducing LMT—RSR observations. Each individual spectrum was analyzed separately. After eliminating bad channels or spectra containing strong ripples, a linear baseline was removed from each spectrum. The final spectrum was obtained by averaging all of the spectra using the  $1/\sigma^2$  weight. The entire reduced spectrum is obtained in units of antenna temperatures scale ( $T_A^*$ ), which have been corrected for atmospheric losses, rear spillover, and scattering. We noted that the spectrum still contains some ripples that were not completely removed by our baseline subtraction procedure. Higher-order baselines did not improve the resulting spectra. A Savitzky–Golay filter (Savitzky & Golay 1964) with a second-order polynomial and 1 GHz width is applied to the full spectrum to reduce low-frequency residual noise (see also Cybulski et al. 2016).

Figure 1 shows the resulting spectrum, which has an overall r.m.s. of 0.1 mK in the 100 GHz spectral region. The final spectrum was converted into main-beam temperatures ( $T_{\text{MB}}$ ) using the relation  $T_{\text{MB}} = \frac{T_A^*}{\eta_{\text{MB}}}$ , where  $\eta_{\text{MB}}$  is the main-beam efficiency of the telescope, whose value for that season was 0.5 at 110 GHz.

Only one feature is detected, with a signal-to-noise ratio (S/N)  $\sim 28$  at 108.705 GHz, which corresponds to the frequency of  $^{12}\text{CO}(1-0)$  molecular line at the redshift of IRAS 17020+4544. It shows a clear asymmetric double-peak structure, with one component peaking at  $-51 \text{ km s}^{-1}$  and the other one peaking at  $+233 \text{ km s}^{-1}$  from the zero of the line.

To reproduce the double-peak structure, we fitted two narrow Gaussian lines to the profile (see Figure 2). The fit with two Gaussian lines shows residuals in the blue wing significant to  $\sim 3\sigma$ .

**Table 1**  
Spectral Fit Parameters for the CO Line Complex

Component	FWHM (km s <sup>-1</sup> )	Centroid (km s <sup>-1</sup> )	Integrated Intensity (mK km s <sup>-1</sup> )	$L_{\text{CO}}$ ( $\times 10^8$ ) (K km s <sup>-1</sup> pc <sup>2</sup> )	$M_{\text{CO}}$ ( $10^8 M_{\odot}$ )	$\alpha$ (CO-to-H <sub>2</sub> ) ( $M_{\odot}$ (K km s <sup>-1</sup> pc <sup>2</sup> ) <sup>-1</sup> )
Broad wing	1112	-660	798 ± 252	3.08 ± 0.97	1.54 ± 0.49	0.5
Line A	213	-51	1390 ± 114	5.37 ± 0.44	4.62 ± 0.38	0.86
Line B	210	233	1171 ± 110	4.53 ± 0.42	3.89 ± 0.36	0.86

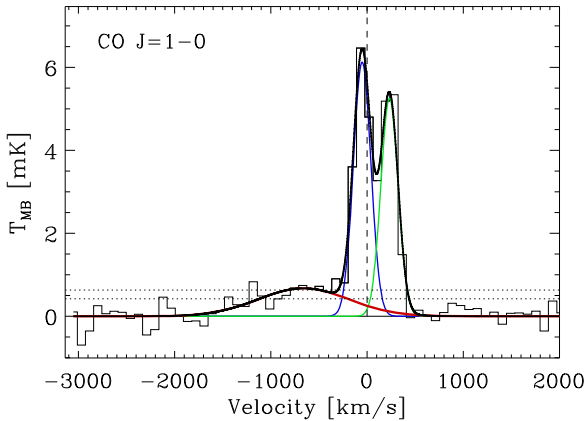


**Figure 2.** Spectrum of the  $^{12}\text{CO}(1-0)$  line in IRAS 17020+4544 obtained with the LMT telescope. The double-peak structure is fitted by two narrow Gaussian components (blue and green), and the line wings are fitted by a very broad Gaussian line (red solid thick line). Dotted horizontal lines mark the  $2\sigma$  and  $3\sigma$  thresholds, and dashed vertical line marks the zero-velocity position. Fit parameters are reported in Table 1.

The CO intensity of each component is reported in Table 1 together with the corresponding molecular gas mass. For both narrow lines, the molecular gas mass is estimated assuming a CO-to-H<sub>2</sub> conversion factor appropriate for ULIRGs (Solomon et al. 1997; Solomon & Vanden Bout 2005). The molecular gas masses estimated in each narrow component are very similar. This finding is compatible with the presence of a molecular disk of material in the galaxy and will be discussed in a later work (A. Oluín-Iglesias 2018, in preparation).

Additionally, the data reveals the presence of a broad feature of the  $^{12}\text{CO}(1-0)$  line. We fitted this excess with an additional Gaussian line that is significantly shifted to the blue with respect to the zero-velocity position. The blue wing extends up to about  $-1500$  km s<sup>-1</sup> with the bulk of velocity peaking at  $-660$  km s<sup>-1</sup>. The resulting simultaneous fit to the three components is shown in Figure 2.

The conversion of the CO luminosity of the broad component into molecular gas mass  $M(\text{H}_2)$  was obtained by assuming a conservative CO-to-H<sub>2</sub> conversion factor  $\alpha = 0.5$ , i.e., 1/10 the Galactic value (Solomon et al. 1987). This is the lowest conversion factor found in different locations of M82 (a typical starburst galaxy), including its molecular outflow (Weiß et al. 2001). We note that this value spans a wide range, and therefore uncertainties in the estimated mass of the molecular gas can vary accordingly. For example, the CO-to-H<sub>2</sub> conversion factor of 2.1 recently estimated by Ciccone et al. (2018) in the local merger NGC 6240 is a factor of 4 higher than the one applied to IRAS 17020+4544. However, we decided to adopt the widely used factor of 0.5 in order to ease comparison with previous results (see Section 4).

The broad component is clearly separated from the double-peak structure, therefore it can be excluded that this feature is arising in a disk-like geometry as the double-peak line. The most viable explanation is that the broad wing of the  $^{12}\text{CO}(1-0)$  line is tracing an outflow of molecular gas whose bulk velocity peaks around  $-660$  km s<sup>-1</sup>.

### 2.1. On the Significance of the Broad Wing in the CO Line

Figure 1 shows that the only prominent broad feature in the entire LMT spectrum is the broad blueshifted component at the base of the double-peaked narrow  $^{12}\text{CO}(1-0)$  line. Although no other broad features are present in the 76–108 GHz and 110–111 GHz continua (see Figure 1), and hence the likelihood of this feature being a spurious detection is negligible, we perform a continuum subtraction simulation to estimate the maximum contribution that any residual baseline could have on the estimated intensity of the broad  $^{12}\text{CO}(1-0)$  line.

We choose at random 2000 frequencies in the 76–108 GHz and 110–111 GHz range to define windows of 20 channels (i.e., the full width at zero intensity (FWZI) of the feature of interest) that represent plausible fiducial continua below the detected broad CO line. We subtract these continua and repeat the fitting procedure as above. Figure 3 shows the resulting impact on the integrated line flux of the broad component. As expected, there is no chance of the broad component disappearing due to residual bandpasses: for all realizations  $L_{\text{CO}(\text{broad})} > 450$  mK km s<sup>-1</sup>. Our originally fitted value of 798 mK km s<sup>-1</sup> is rarely exceeded, and this could be indicative of smaller-scale residuals still present in the continuum or the added contribution of faint lines. Our most conservative estimation of the broad line intensity is, hence, given by the median of the distribution in Figure 3:  $L_{\text{CO}(\text{broad})} = 690$  mK km s<sup>-1</sup>, with a 68% confidence interval in the 590–760 mK km s<sup>-1</sup>.

We are therefore confident that the detection of the line broad wing is statistically robust and that its astrophysical properties are genuinely derived in this Letter.

## 3. The Outflows in IRAS 17020+4544

### 3.1. The Molecular Outflow

The 20 arcsec resolution of the LMT at 110 GHz does not allow us to infer the spatial scale of the CO wind, it only provides an upper limit of 23 kpc at the distance of IRAS 17020+4544. Therefore, accounting for the beam size, it is reasonable to say that the present LMT observation can trace molecular gas up to  $\sim 20$  kpc. Considering that an average AGN lifetime cycle corresponds to  $10^{6-7}$  years, the spatial extension that molecular gas outflowing at the observed velocity can swipe during the AGN life corresponds to about 0.67–6.7 kpc. These numbers are also in excellent agreement with the dynamical timescale inferred by considering that the

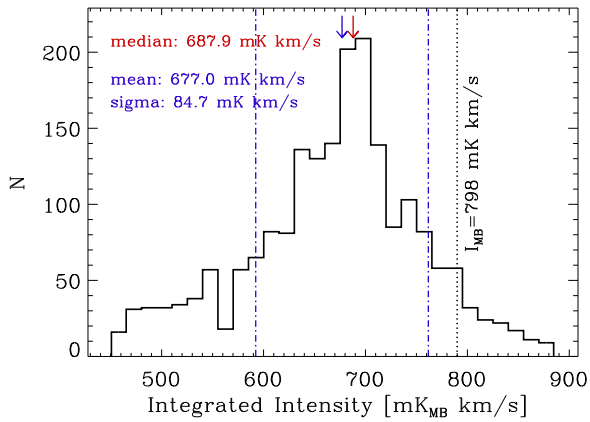


**Figure 3.** Comparison between the best-fit value of the flux in the broad wing of the CO line measured on the LMT spectrum (dotted line) and the results of 2000 trials where the broad line is fitted after randomly subtracting continuum portions of 20 channels extracted from the 76–108 GHz and 110–111 GHz continuum interval.

molecular gas is moving at a bulk velocity of  $-660 \text{ km s}^{-1}$ . Therefore, the dynamical timescale  $T_{\text{dyn}}$  of  $10^6$  years for the outflow to propagate out of the nucleus corresponds to a radius  $R \sim 0.67 \text{ kpc}$ . At this distance, assuming spherical symmetry and that the outflow is moving at the bulk velocity of  $-660 \text{ km s}^{-1}$ , the estimated mass outflow rate is  $\dot{M}_{\text{[CO]}} = 3 \frac{M_{\text{H}_2} \times v_{\text{out}}}{R}$ , which yields a mass loss of  $\sim 480 M_{\odot} \text{ yr}^{-1}$ . If we consider the higher spatial scale of  $6.7 \text{ kpc}$ , which corresponds to an AGN lifetime of  $10^7$  years, the mass outflow rate decreases to  $48 M_{\odot} \text{ yr}^{-1}$ . These numbers are estimated assuming that the velocity of the outflow is measured as the centroid of the broad line in the LMT spectrum (see Table 1), i.e., as the shift between the peaks of the narrow and broad component. This measurement may be affected by our limited knowledge of the geometry of the outflow, particularly of the inclination of the outflow with respect to our line of sight.

In this regard, the estimate of the velocity proposed by Rupke & Veilleux (2013)  $v_{\text{out}} = \text{velocity shift}_{\text{broad}} + 2\sigma_{\text{broad}}$ , where  $\sigma_{\text{broad}} = \frac{\text{FWHM}_{\text{broad}}}{2.35}$ , shall be less affected by the outflow geometry. Hence, we provide the estimate of the mass loss rate for the outflow traveling at  $v_{\text{out}} = -1600 \text{ km s}^{-1}$  and at a distance of  $0.67 \text{ kpc}$ . This estimate, which yields  $\dot{M}_{\text{[CO]}} = 1162 M_{\odot} \text{ yr}^{-1}$ , can be taken as a maximum uncertainty on the amount of mass that the AGN is capable of expelling via molecular outflow. All of these rates are estimated assuming a uniform distribution of the molecular gas in a spherical geometry with radius  $R$ .

The force or momentum flux of this wind is related to the velocity with which the gas is pushed outward i.e., the outflow velocity, therefore it is equivalent to  $\dot{P}_{\text{out}} = \dot{M}_{\text{out}} \times v_{\text{out}}$ . Assuming that the gas is outflowing at bulk velocity of  $-660 \text{ km s}^{-1}$  and assuming that the gas is still confined on the smaller spatial scale of  $0.67 \text{ kpc}$ , this would yield  $\dot{P}_{\text{[CO]}} = \dot{M}_{\text{[CO]}} \times v_{\text{[CO]}}$ , i.e.,  $\dot{P}_{\text{[CO]}} \sim 2 \times 10^{36} \text{ cm g s}^{-2}$ . Considering the source bolometric luminosity,  $L_{\text{bol}} = 5 \times 10^{44} \text{ erg s}^{-1}$ , the force of the radiation pressure can be expressed as  $\dot{P}_{\text{rad}} = \frac{L_{\text{bol}}}{c} = 1.7 \times 10^{34} \text{ cm g s}^{-2}$ , and conversely, the ratio of the force of the molecular outflow versus the force of the radiation would be  $\frac{\dot{P}_{\text{[CO]}}}{\dot{P}_{\text{rad}}} \sim 117$ . We remark

that the bolometric luminosity here considered was estimated accordingly to Longinotti et al. (2015) and by assuming a conservative low bolometric correction ( $k = 10$ ; see Marconi et al. 2004). If we relax the assumption on the spatial scale maintaining the bulk outflow velocity, we obtain  $\dot{M}_{\text{[CO]}} = 48 M_{\odot} \text{ yr}^{-1}$  and thus  $\dot{P}_{\text{[CO]min}} = 2 \times 10^{35} \text{ cm g s}^{-2}$  and  $\frac{\dot{P}_{\text{[CO]min}}}{\dot{P}_{\text{rad}}} \sim 11$ . If we now consider the higher outflow velocity of  $-1600 \text{ km s}^{-1}$ , the resulting momentum flux of the outflow is boosted to  $\dot{P}_{\text{[CO]max}} = 1.14 \times 10^{37} \text{ cm g s}^{-2}$ , which leads to a ratio of  $\frac{\dot{P}_{\text{[CO]max}}}{\dot{P}_{\text{rad}}} \sim 670$  with respect to the momentum of the AGN radiation.

### 3.2. Relation with the X-Ray Outflow

The detailed properties of the X-ray wind detected in IRAS 17020+4544 are reported in Longinotti et al. (2015) and Sanfrutos et al. (2018). We defer the reader to these publications for all of the details on the *XMM-Newton* data analysis and results.

Out of the multiple components that were revealed in the X-ray wind, only one was found that was massive enough to expel the gas and trigger negative feedback in the galaxy. The column density and outflow velocity of this X-ray wind were  $N_{\text{H}} \sim 10^{23.9} \text{ cm}^{-2}$  and  $v_{\text{out}} = 27,200 \pm 300 \text{ km s}^{-1}$  (Longinotti et al. 2015). As outlined in Section 3.1, the momentum flux of this wind is estimated through the outflow velocity and the mass flux expelled by the wind  $\dot{P}_X = \dot{M}_X \times v_{\text{out}}$ .

The mass and energy outflow rates of the X-ray wind were estimated and parametrized in terms of the wind covering factor:  $\dot{M}_{\text{out}} \sim 0.26 C_f M_{\odot} \text{ yr}^{-1}$  and  $\frac{\dot{E}}{L_{\text{BOL}}} = 11\% C_f \text{ erg s}^{-1}$ . The X-ray data presented in Longinotti et al. (2015) did not allow an exact estimate of the geometry and covering factor of the wind. However, we note that the X-ray wind plausibly originates at accretion disk scale in a conical geometry (e.g., Krongold et al. 2007) and that it has to be sufficiently powerful to push the molecular gas, therefore its covering factor cannot be much lower than 1. We then assume that  $C_f$  may vary in the 0.5–1 range.

Under this assumption, the X-ray wind momentum flux is  $\dot{P}_{\text{[X]}} = (2.15\text{--}4.3) \times 10^{34} \text{ cm g s}^{-2}$ . Considering the force of the radiation pressure as done in Section 3.1 for the molecular outflow, the ratio of the X-ray wind force versus the radiation force is estimated to be  $\frac{\dot{P}_{\text{[X]}}}{\dot{P}_{\text{rad}}} = 1.87 \pm 0.62$ . Remarkably, these error bars are dominated by the uncertainties on the covering factor of the wind rather than by its outflow velocity, as the availability of grating spectroscopy (Longinotti et al. 2015) allowed the shift of the absorption lines position to be measured to a higher precision.

## 4. Discussion

The results obtained in the two previous sections are summarized in Figure 4, which is adapted from Feruglio et al. (2015) and which includes the uncertainties on the outflow distance and the outflow velocity described in Section 3.1. This plot compares the prediction for the behavior of an energy-conserving wind where the outer molecular outflow is driven by a subrelativistic wind arising at a more inner scale, as postulated by several authors (Faucher-Giguère & Quataert 2012; Zubovas & King 2012, and references therein). So far, this theory has been corroborated by

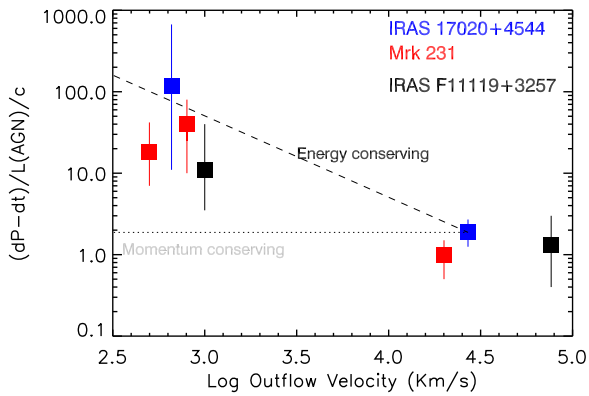


**Figure 4.** Plot adapted from Figure 16 in Feruglio et al. (2015) showing the force of the molecular and X-ray phases of the wind plotted against their outflow velocities for the three sources where this relation has been observed. The wind force is expressed in terms of the ratio between the flux of the momentum of the wind ( $\dot{P}_{\text{outflow}}$ ) divided by the force of the radiation  $\dot{P}_{\text{rad}}$ . The black dashed line marks the prediction for an energy-conserving outflow i.e.,  $\dot{P}_{\text{CO}}/\dot{P}_{\text{X}} = v_{\text{out,X}}/v_{\text{out,CO}}$  in IRAS 17020+4544. The gray dotted line marks the prediction for momentum-conserving outflows.

observations obtained for the two ULIRGs Mrk 231 (Feruglio et al. 2015) and IRAS F11119+3257 (Tombesi et al. 2015), which provide the only two examples of AGN where an X-ray ultra-fast wind and a molecular outflow are observed with momentum loads typical of energy-conserving outflows.

The result obtained for IRAS 17020+4544 provides a third indication for the existence of such energy-conserving winds. The uncertainties in the estimates of the mass outflow rates and the wind spatial extent do not allow us to reduce the errors in the calculation of the mutual momentum load of the outflows detected in the X-ray and in the millimeter bands plotted in Figure 4. It is remarkable, however, that the pattern of the outflow force is fairly inconsistent with a wind that conserves its momentum even after accounting for every source of uncertainties.

This additional piece of evidence for an energy-conserving wind that propagates through the galaxy after undergoing a momentum boost supports the scenario in which powerful AGN outflows are capable of producing feedback on the host galaxy and regulate star formation as proposed in earlier works (Tombesi et al. 2015, and references therein).

We here anticipate that the outflow properties inferred from the LMT spectrum are fully supported by proprietary data recently obtained at the NOEMA interferometer that will be presented elsewhere. Interferometry data have been shown to be a powerful tool to provide refined constraints on the properties of outflowing molecular gas (e.g., Feruglio et al. 2010, 2015); therefore, in the future we expect to mitigate the source of uncertainties in the error bars of Figure 4 for IRAS 17020+4544.

#### 4.1. A Multi-phase Outflow in a Seyfert Galaxy at Moderate Luminosity?

The case of IRAS 17020+4544, though, bears some important differences from the AGN reported in Figure 4.

The bolometric luminosity of the two ULIRGs described in Section 4 is more typical of powerful AGN, being  $5 \times 10^{45} \text{ erg s}^{-1}$  for Mrk 231 and  $\sim 10^{46} \text{ erg s}^{-1}$  for IRAS F11119+3257 (respectively, Feruglio et al. 2015; Tombesi et al. 2015), i.e., at least an order of magnitude larger than in IRAS 17020+4544. Moreover, as noted already in Longinotti et al. (2015), the

infrared luminosity of  $L_{\text{FIR}} = 1.05 \times 10^{11} L_{\odot}$  is not high enough to classify the source as an ULIRG.

On the contrary, this AGN is hosted by a barred spiral galaxy with no sign of interaction or disturbed morphology (A. Olgún-Iglesias 2018, in preparation); therefore, the result presented here corroborates the evidence that feedback mechanisms typical of gas-rich galaxies at an early evolutionary stage can also arise in lower-luminosity spiral galaxies.

Remarkably, IRAS 17020+4544 also shows peculiar radio properties (Giroletti et al. 2017), among which is an elongated structure produced by synchrotron emission on a 10 pc scale. This structure is estimated to be moving at a velocity consistent with the X-ray outflows, and it might be resolved in a jet in future very-long-baseline interferometry observations at higher resolution. If confirmed, the presence of such a “jet” may represent the signature left by the shock of the inner X-ray outflow with the ambient gas that is postulated in several models of galactic outflows (e.g., Zakamska & Greene 2014; Nims et al. 2015), which attempt to link synchrotron emission in radio-quiet sources with galaxy scale outflows.


Further hints to the presence of a shocked outflow in this source come from a recent analysis of the connection of the X-ray slow and fast wind (Sanfrutos et al. 2018; Longinotti 2018), and refined constraints on the energy-conserving scenario are to be expected once IRAS 17020+4544 is observed in the ultraviolet (UV) band by the Cosmic Origins Spectrograph on board the *Hubble Space Telescope* (P.I.: Y. Krongold) to search for a UV counterpart of the nuclear wind.

A confirmation of this hypothesis would convert IRAS 17020+4544 in a unique laboratory to study all phases of an energy-driven outflow.

The authors thank the anonymous referee for the insightful comments and suggestions that have significantly increase the clarity of our manuscript. All authors acknowledge technical support from the LMT team at INAOE and at UMASS. A.L.L. acknowledges support through Catédra CONACyT n.323. This work was partially supported by CONACyT research grants 151494 and 280789. Y.K. acknowledges support from PAPIIT grant IN06518 from UNAM. C.F. acknowledges support from the European Union Horizon 2020 Research and Innovation Programme under the Marie Skłodowska-Curie grant agreement No 664931. J.K. acknowledges financial support from the Academy of Finland, grant 311438. L.A.Z. acknowledges financial support from DGAPA, UNAM, and CONACyT, México. D.D. acknowledges support through grant IN108716, from PAPIIT, UNAM and grant 221398 from CONACyT. I.C.G. acknowledges support from DGAPA-UNAM (Mexico) grant IN113417. Funding is acknowledged via CONACyT grants CB-183013-F (O.V.), CB2016-81948 (I.A.), and CB-2016-01-286316 (A.L.L.).

#### ORCID iDs

A. L. Longinotti <https://orcid.org/0000-0001-8825-3624>  
 O. Vega <https://orcid.org/0000-0002-2852-9737>  
 Y. Krongold <https://orcid.org/0000-0001-6291-5239>  
 I. Aretxaga <https://orcid.org/0000-0002-6590-3994>  
 M. Yun <https://orcid.org/0000-0001-7095-7543>  
 V. Chavushyan <https://orcid.org/0000-0002-2558-0967>  
 C. Feruglio <https://orcid.org/0000-0002-4227-6035>  
 A. Montaña <https://orcid.org/0000-0003-4229-381X>  
 M. Giroletti <https://orcid.org/0000-0002-8657-8852>

J. Kotilainen  <https://orcid.org/0000-0003-0133-7644>  
 F. Panessa  <https://orcid.org/0000-0003-0543-3617>  
 L. A. Zapata  <https://orcid.org/0000-0003-2343-7937>  
 I. Cruz-Gonzalez  <https://orcid.org/0000-0002-2653-1120>  
 D. Rosa-Gonzalez  <https://orcid.org/0000-0003-1327-0838>  
 A. Carramiñana  <https://orcid.org/0000-0002-8553-3302>  
 E. Costantini  <https://orcid.org/0000-0001-8470-749X>  
 M. Santos-Lleo  <https://orcid.org/0000-0001-5948-8360>

## References

- Carniani, S., Marconi, A., Maiolino, R., et al. 2015, *A&A*, **580**, A102  
 Cicone, C., Maiolino, R., Sturm, E., et al. 2014, *A&A*, **562**, A21  
 Cicone, C., Severgnini, P., Papadopoulos, P. P., et al. 2018, *ApJ*, **863**, 143  
 Cybulski, R., Yun, M. S., Erickson, N., et al. 2016, *MNRAS*, **459**, 3287  
 Di Matteo, T., Springel, V., & Hernquist, L. 2005, *Natur*, **433**, 604  
 Doi, A., Asada, K., & Nagai, H. 2011, *ApJ*, **738**, 126  
 Erickson, N., Narayanan, G., Goeller, R., & Grosslein, R. 2007, in ASP Conf. Ser. 375, From Z-Machines to ALMA: (Sub)Millimeter Spectroscopy of Galaxies, ed. A. J. Baker et al. (San Francisco, CA: ASP), 71  
 Faucher-Giguère, C.-A., & Quataert, E. 2012, *MNRAS*, **425**, 605  
 Feruglio, C., Maiolino, R., Piconcelli, E., et al. 2010, *A&A*, **518**, L155  
 Feruglio, C., Fiore, F., Carniani, S., et al. 2015, *A&A*, **583**, A99  
 Fiore, F., Feruglio, C., Shankar, F., et al. 2017, *A&A*, **601**, A143  
 Giroletti, M., Panessa, F., Longinotti, A. L., et al. 2017, *A&A*, **600**, A87  
 Gofford, J., Reeves, J. N., Tombesi, F., et al. 2013, *MNRAS*, **430**, 60  
 Harrison, C. M., Alexander, D. M., Mullaney, J. R., & Swinbank, A. M. 2014, *MNRAS*, **441**, 3306  
 Hopkins, P. F., & Elvis, M. 2010, *MNRAS*, **401**, 7  
 Hughes, D. H., Jáuregui Correa, J.-C., Schloerb, F. P., et al. 2010, *Proc. SPIE*, **7733**, 773312  
 King, A. R. 2010, *MNRAS*, **402**, 1516  
 Krongold, Y., Nicastro, F., Elvis, M., et al. 2007, *ApJ*, **659**, 1022  
 Longinotti, A. L., Krongold, Y., Guainazzi, M., et al. 2015, *ApJL*, **813**, L39  
 Longinotti, A. L. 2018, arXiv:1808.01043  
 Marconi, A., Risaliti, G., Gilli, R., et al. 2004, *MNRAS*, **351**, 169  
 Nardini, E., & Zubovas, K. 2018, *MNRAS*, **478**, 2274  
 Nims, J., Quataert, E., & Faucher-Giguère, C.-A. 2015, *MNRAS*, **447**, 3612  
 Rupke, D. S. N., & Veilleux, S. 2013, *ApJ*, **768**, 75  
 Sanfrutos, M., Longinotti, A. L., Krongold, Y., et al. 2018, *ApJ*, in press (arXiv:1810.07714)  
 Savitzky, A., & Golay, M. J. E. 1964, *AnaCh*, **36**, 1627  
 Solomon, P. M., Rivolo, A. R., Barrett, J., & Yahil, A. 1987, *ApJ*, **319**, 730  
 Solomon, P. M., Downes, D., Radford, S. J. E., & Barrett, J. W. 1997, *ApJ*, **478**, 144  
 Solomon, P. M., & Vanden Bout, P. A. 2005, *ARA&A*, **43**, 677  
 Tombesi, F., Cappi, M., Reeves, J. N., & Braito, V. 2012, *MNRAS*, **422**, L1  
 Tombesi, F., Meléndez, M., Veilleux, S., et al. 2015, *Natur*, **519**, 436  
 Veilleux, S., Meléndez, M., Sturm, E., et al. 2013, *ApJ*, **776**, 27  
 Zakamska, N. L., & Greene, J. E. 2014, *MNRAS*, **442**, 784  
 Zubovas, K., & King, A. 2012, *ApJL*, **745**, L34  
 Weiß, A., Neininger, N., Hüttemeister, S., & Klein, U. 2001, *A&A*, **365**, 571  
 Wisotzki, L., & Bade, N. 1997, *A&A*, **320**, 395